Configurational anisotropy and control of magnetic vortex chirality in arrays of circular $Ni_{80}Fe_{20}$ nanoscale dots

S. Jain, Y. Ren, and A. O. Adeyeye*
Information Storage Materials Laboratory, Department of Electrical and Computer Engineering, National University of Singapore, Singapore 117576, Singapore

N. Singh
*Institute of Microelectronics, A*STAR (Agency for Science, Technology and Research), Singapore 117685, Singapore*
(Received 21 May 2009; revised manuscript received 2 September 2009; published 5 October 2009)

We present the experimental investigation and numerical analysis of the magnetostatic energy of ferromagnetic circular dots arranged in three different lattice geometries. We show that by varying the lattice arrangement, configurational anisotropy, which is significantly affected by the direction of the external magnetic field, can be induced. Depending on the coupling mechanism (ferromagnetic/antiferromagnetic) between the neighboring dots in the lattice, different combinations of chiralities in the vortex state can be obtained.

DOI: 10.1103/PhysRevB.80.132401 PACS number(s): 75.60.Jk

Magnetostatic interactions in coupled nanodots have attracted much attention in recent years.[1,2] Fundamentally, such systems are well suited for direct comparison between theoretical predictions and experimental observations. Due to the advancements in nanofabrication techniques,[3] it is now possible to precisely control the geometry, size, and interdot spacing in magnetic nanodots. Depending on the geometrical size of the dot, either a stable single-domain configuration can be obtained at remanence or a "curling magnetization distribution," also referred to as a magnetic vortex can be observed. Compared to single-domain states, magnetic vortices have much lower stray fields due to flux closure configuration and can thus be formed as an equilibrium state or ground state at remanence.[4] Therefore, having stable and controlled vortex chirality is a key requirement for the successful implementation of ferromagnetic (FM) nanostructures in logic devices and memory cells. In general, the magnetization reversal process is determined by a combination of all the energy terms including exchange, magnetocrystalline anisotropy, and magnetostatic contributions. When FM dots are placed closed to each other such that their side magnetic charges begin to interact, the resultant dipole coupling energy can dominate their magnetization reversal mechanism and in turn affect the total magnetostatic energy of the system. Controlling the vortex chirality in such cases consequently becomes even more challenging.

In recent years, there has been substantial work reported on the stability of the vortex state with regard to shape and size in an array of both isolated and coupled magnetic dots.[4–16] For instance, Natali *et al.*[7] studied two-dimensional arrays of densely packed Co dots and showed the existence of dipolar interactions between single-domain dots and vortex state dots. Similarly, Guslienko *et al.*[8] and Novosad *et al.*[9] have investigated the effect of magnetostatic coupling on the nucleation and annihilation fields in one-dimensional and two-dimensional arrays of permalloy dots. Furthermore, Cowburn[17] showed that by arranging the permalloy dots in a linear chain and by engineering the anisotropy of each dot, antiferromagnetic (AFM) arrangement can be obtained in the dots. However, there has been no work reported so far on the manipulation of the magnetostatic energy of a the system consisting of ferromagnetic dots arranged in specific lattice geometries, which in turn determines the vortex chirality of each dot. Such control of magnetostatic coupling in nanodots is crucial for the design of future spintronic logic devices[18,19] and storage memory cells.[20]

In this Brief Report, we investigate how configurational anisotropy (resulting from the lattice arrangements of dots) and field orientation affects the vortex chiralities in FM circular dots when they are arranged in different lattice configurations. By arranging the dots in specific lattice geometries, configurational anisotropy can be induced, which favors a preferential mode of magnetization reversal. We have systematically mapped this effect by varying the direction of the applied field. The results shown in this work are specifically important for storing different combinations of bit patterns as one cell, in contrast to single element memory cells.

Periodic arrays of circular dots of diameter 600 nm in three different configurations were fabricated over an area of 100×100 μm^2 on silicon substrates using deep ultraviolet lithography at 248 nm wavelength followed by the lift-off process. The edge to edge spacing s between the dots was varied from 55 to 600 nm, respectively. $Ni_{80}Fe_{20}$ of thickness (t_{NiFe}) 80 nm was deposited using electron-beam evaporation at a rate of 0.2 Å/s. Details of the fabrication process are described elsewhere.[21] Figure 1(a) shows the representative scanning electron micrographs of the three lattice geometries for both closely spaced dots ($s=55$ nm) and isolated dots ($s=600$ nm). Hysteresis loops were recorded using a focused magneto-optical Kerr effect (MOKE) setup with a 5 μm spot size and external field applied in longitudinal geometry at room temperature. Magnetic force microscopy (MFM) imaging was performed in the phase detection mode using commercial CoCr coated Si cantilever tips magnetized along the tip axis.

In order to understand the underlying physics we first performed numerical calculations based on "rigid" vortex model proposed by Guslienko *et al.*[8] Figure 1(b) shows the lattice system of the nanodots considered for three different configurations. The center-to-center distance is defined as $D \equiv Rd$ for both the x and y axes, where R is the radius of the dot and d is the nondimensional separating distance.

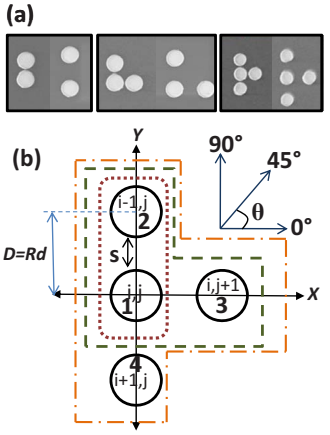

FIG. 1. (Color online) (a) Scanning electron microscopy micrographs of circular dot in three different lattice configurations for both closely spaced dots (s=55 nm) and isolated dots (s=600 nm), and (b) schematic illustration of the dot geometries in coordinate system.

In a system of coupled dots, each vortex magnetostatically interacts with each other due to the magnetic charges $\sigma(\varphi_i)(i=1,2)$ emerging on the side surfaces of the dots when the vortex core shifts from the center. The magnetostatic energy between the side surfaces of two dots can be thus written as

$$W_{int}(a_1,a_2)=\frac{\mu_0 M_s^2 R^3}{8\pi}\int\frac{dZ_1 dZ_2 d\varphi_1 d\varphi_2 \sigma(\varphi_1)\sigma(\varphi_2)}{K(\varphi_1,Z_1,\varphi_2,Z_2)}, \quad (1)$$

where $K(\varphi_1,Z_1,\varphi_2,Z_2)=[d^2+2d(\cos\varphi_2-\cos\varphi_1)+2-2\cos(\varphi_2-\varphi_1)+(Z_2-Z_1)^2]^{1/2}$. The integration in Eq. (1) runs from 0 to t_{NiFe}/R in Z_1 and Z_2 and from 0 to 2π in φ_1 and φ_2, where t_{NiFe} is the dot thickness. Since the core radius of the vortex is small enough compared with the disk radius R, the interactions between the charge distribution on the top and bottom surfaces of the two disks are negligible.

The interaction energy due to the magnetostatic coupling of the two-dot system was subsequently calculated using Eq. (1). Figure 2(a) shows the variation in the magnetostatic energy as a function of the spacing s between the two dots as a function of the external magnetic field orientation (θ). For θ=0°, the calculated magnetostatic energy yields positive values, whereas for θ=45° and 90° it generates negative values. To fully understand the spin configurations, we also performed micromagnetic simulations using object-oriented micromagnetic framework (OOMMF).[22] Standard parameters of $Ni_{80}Fe_{20}$ were used for simulations (M_s=860 kA/m, A=1.3 μerg/cm, α=0.5, and cell size=5 nm×5 nm). Figure 2(b) shows the spin configuration of the two dots at remanence for θ=0°, 45°, and 90° when s=55 nm. We observed that the direction of the external field strongly influences the chirality of the vortex state which in turn determines the spin configuration of the entire system. For θ=0°, the vortex core nucleates at the edge position perpendicular to the field direction such that the chirality in the two dots is antiparallel. This results in the magnetic moments at the edges of the interacting dots pointing in the same direction,

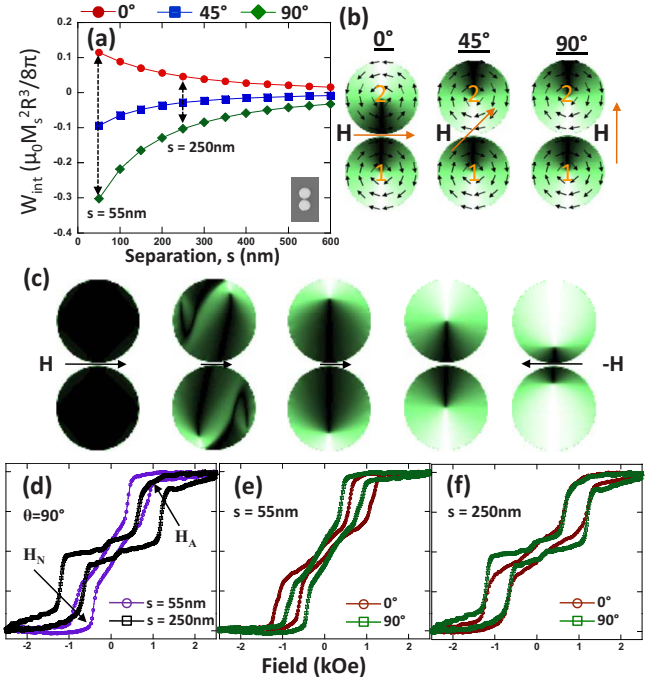

FIG. 2. (Color online) (a) Variation in the interaction energy $W_{int(2\ dot)}$ as a function of the interdot spacing s for θ=0°, 45°, and 90°, and t_{NiFe}=80 nm. (b) Simulated spin states of two dots for s=55 nm and t_{NiFe}=80 nm as a function of field orientation (θ). (c) Systematic evolution of magnetization distribution in two-dot lattice geometry for θ=0° starting from positive saturation to negative saturation. (d) M-H loops for the same dot geometry at θ=90° and s=55 nm and 250 nm. (e) M-H loops for s=55 nm at θ=0° and 90°. (f) M-H loops for s=250 nm at θ=0° and 90°.

showing FM coupling. This observation is also supported by the numerical calculations in the form of positive values for the interaction energy $W_{int(2\ dot)}$. To have a clear understanding of the spin evolution in a dot pair, Fig. 2(c) depicts the various spin configurations at different magnitudes of applied field when θ=0°. For θ=90°, however, the vortex state in the two interacting dots favor same vortex chirality, resulting in antiparallel alignment of magnetic moments at the edges of the dots and thus exhibits AFM coupling. The negative values of $W_{int(2\ dot)}$ for θ=90° also support similar argument. This signifies that the direction of the external magnetic field determines the chirality of the vortex state in two interacting FM dots, i.e., the two dots can either have clockwise or anticlockwise vortex chirality in both of them or have clockwise chirality in one dot while the other vortex rotates in anticlockwise direction. This phenomenon may be particularly interesting for spintronic logic devices where the input direction of magnetic field can generate outputs of parallel or antiparallel vortex chiralities in the magnetic elements. As expected, when the separation between the two dots increases, the magnetostatic energy decreases and converges to zero for all the applied field directions.

Shown in Fig. 2(d) are the M-H loops obtained using focused MOKE magnetometry for s=55 and 250, for field applied along θ=90°. The interaction energy corresponding to these two separations is also marked in Fig. 2(a). It is clearly observed that there exists a weak magnetostatic inter-

action between dots with $s=250$ nm. For the most widely spaced dots corresponding to $s=600$ nm, it was difficult to obtain MOKE signal due to sensitivity limitations of the system. Comparing the M-H loops for the two interdot spacings, we observed that the magnetization reversal process (including nucleation $[H_N]$ and annihilation $[H_A]$ of vortex cores) are significantly affected. Consequently, for $s=55$ nm, $H_N=-466$ Oe, and $H_A=1016$ Oe while for $s=250$ nm, $H_N=-766$ Oe, and $H_A=1383$ Oe. This increase in H_N and H_A with increasing interdot spacing can be attributed to the decreased magnetostatic coupling between the two dots. This results in easy nucleation of the vortex core when the external magnetic field is reduced from saturation. Further, magnetization curves were obtained for both $s=55$ and 250 nm at different values of θ. Figure 2(e) shows the magnetization responses for $s=55$ nm when the external magnetic field is applied at an angle of $\theta=0°$ and 90°. We observed that the nucleation of the vortex core starts at a lower field value for $\theta=90°$ (−466 Oe) as compared to $\theta=0°$ (−683 Oe). Similarly, the annihilation of the vortex core takes place at a smaller field value for $\theta=90°$ (1016 Oe) as compared to $\theta=0°$ (1289 Oe). The corresponding M-H loops for $s=250$ nm are shown in Fig. 2(f). As expected, there is no significant difference in the nucleation field or the annihilation field for $\theta=0°$ and 90°. However, the magnetization reversal process which constitutes the propagation of vortex core from one edge of the dot to the other is relatively distinguishable. The decrease in magnetization at H_N is more abrupt for $\theta=90°$ as compared to 0°. This difference can be attributed to the fact that $\theta=90°$ is the preferred orientation in which the vortex core readily propagates from one edge of the dot to the other. This is attributed to the existing small coupling energy between the two dots since the separation s between them is still less than the radius of the dot. The above-discussed experimental results show that there exists an extrinsic anisotropy in the lattice arrangement which clearly distinguishes the magnetization reversal behavior of the dots when the external magnetic field is applied in two different directions. This concept of "configurational" anisotropy was introduced by Cowburn *et al.*[23] for isolated square nanomagnets. We have successfully shown the presence of this phenomenon in interacting nanomagnets since there exists a preferred field direction in which the vortex core nucleates and annihilates easily at a smaller field value as compared to the other field direction. These results show that even though isolated circular dots do not exhibit any shape anisotropy with respect to the direction of the external field, by arranging them in different lattice geometries, configurational anisotropy which is strongly dependent on the applied field direction can still be induced.

After establishing the fact that the vortex chirality in a two-dot system can be fully controlled by the external magnetic field direction, we further investigate the effect of lattice arrangements in three- and four-dot geometries. Shown in Fig. 3(a) is magnetization response of three-dot lattice arrangement with $s=55$ nm, when $\theta=0°$ and 45°. For $\theta=0°$, the magnetization reversal process undergoes nucleation and annihilation processes in two steps. The spin states obtained from OOMMF simulations corresponding to the two-step nucleation process (H_1 and H_2) are depicted as insets in Fig.

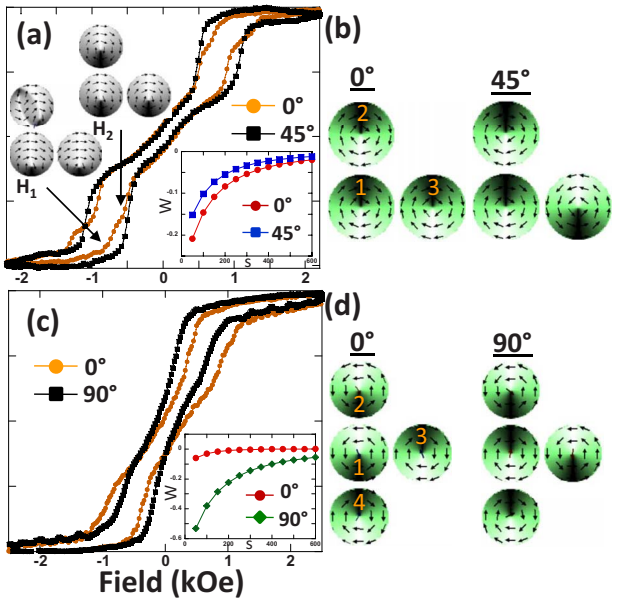

FIG. 3. (Color online) (a) M-H loops for the three-dot lattice geometry for $s=55$ nm, $t_{NiFe}=80$ nm, and $\theta=0°$ and 45°. Corresponding spin states of the same geometry is shown in (b). Similarly, (c) and (d) shows the M-H loops and simulated spin states for four-dot lattice geometry at $\theta=0°$ and 90°. The insets in (a) and (c) are the variations in interaction energies as a function of the spacing between the dots for different values of θ.

3(a). H_1 is the state in which two out of three dots have vortex nucleation at the edges while the third one is still in "S" shape configuration. H_2 marks the onset of the vortex nucleation in the remaining dot as well. Similar two-step reversal process is also true for the annihilation process where the vortex core has fully annihilated from two dots in the first step and from the third dot in the second step. For $\theta=45°$, however, the nucleation and annihilation processes take place at the same time in the entire dot lattice. This direction of the applied field is also the preferred orientation since the magnitude of H_N and H_A is lower as compared to 0°. The variation in the interaction energy as a function of the separation s between the dots is also shown as inset in Fig. 3(a). The total interaction energy of the system is found to be negative for both orientations. Figure 3(b) shows the simulated spin configuration for $\theta=0°$ and 45° at remanence. Due to the induced configurational anisotropy in the system, there exists an obvious symmetry in the reversal process for $\theta=0°$ and 90°. For $\theta=0°$, dots **1** and **3** [as indicated in Fig. 1(b)] try to achieve parallel chiralities in the vortex state as explained above for the two-dot system. At the same time, dots **1** and **2** also try to attain antiparallel configuration of the vortex state. However, there exists another coupling energy between the dots **2** and **3** which experiences the effect of external field at an angle of 45°. The resultant of all the competing energies is that every dot now has the same chirality exhibiting strong AFM coupling (also evidenced by the negative values of W). On the other hand, for $\theta=45°$, out of the three dots, two have the same chirality. Since one of the dot pair experiences ferromagnetic coupling, the magnitude of interaction energy for 45° is less than that of 0°. Therefore, it is possible to have four different combinations

of the vortex chirality depending on the direction of the external magnetic field.

Figure 3(c) shows the magnetization reversal behavior in four-dot lattice geometry for $\theta=0°$ and 90°. Again, due to the induced configurational anisotropy, 90° is the easy axis where nucleation and annihilation of vortex cores takes place at lower field values when compared to 0°. Moreover, we also observed that the magnetization reversal behavior in four-dot lattice geometry is noticeably different from that of two-dot and three-dot configurations. For four-dot lattice geometry, there is no abrupt change in magnetization at H_N. There is only gradual change in magnetization observed beginning from the nucleation field toward the annihilation field. This is true for both $\theta=0°$ and 90° and can be attributed to the strong-interaction fields experienced by each dot in the lattice which forbids the collective nucleation of vortex core inside the dots. This implies that the nucleation of vortex core at the edges of the dots takes place at different field values, thereby changing the magnetization gradually. The plateau region observed in Fig. 3(a) which corresponds to the propagation of vortex core from one edge of the dot to the other is difficult to distinguish in Fig. 3(c). This is because when the nucleation is taking place in one of the dots, the already nucleated vortex core of neighboring dot would probably be propagating to the opposite edge. This is also true because the symmetry of the system has been disturbed by placing dot **3** near dot **1** in a linear chain of dots **1**, **2**, and **4**. The inset in Fig. 3(c) shows the calculated interaction energy of the entire system as a function of the spacing between the dots. The corresponding spin states at remanence for $\theta=0°$ and 90° are shown in Fig. 3(d). Each dot pair experiences different type of coupling depending on the direction of the external field. The resultant is the different combination of chiralities in the lattice geometry. To further corroborate the obtained results, Fig. 4 shows the MFM images for the three configurations ($s=55$ nm and $t_{NiFe}=80$ nm) at remanence, after saturating the structures at +4 kOe and bringing them back to zero. The saturation field was applied at $\theta=0°$. The images reveal the direct evidence of vortex formation at remanence which were also predicted using micromagnetic simulations. The bright contrast (red or yellow) of the vortex core (indicated by arrow) is easily noticeable in the center of each nanodot. Different contrasts of the vortex core represent different polarization vectors of the vortex core. For two-dot geometry, the two polarization vectors point in the same direction (upward or downward). However, in three-dot lattice geometry, due to additional coupling of dot **3**, dots **1** and **2** now have opposite polarization vectors. Similar is the observation for four-dot geometry. These results are the direct consequences of the strong interplay between the coupled dots which results in different polarization vectors of the vortex cores. We have therefore shown that by using an appropriate choice of the field orientation, particular lattice geometry can yield a specific chirality combination which may be very useful for magnetic logic devices.

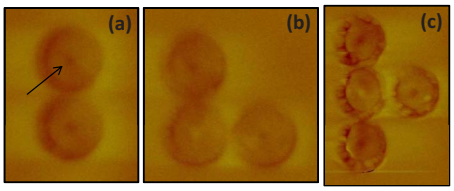

FIG. 4. (Color online) MFM images for (a) two-dot, (b) three-dot, and (c) four-dot lattice geometries at remanence, after saturating the structures at +4 kOe. The saturating field was applied at $\theta=0°$.

To conclude, we have investigated theoretically and experimentally the effect of magnetostatic coupling between the circular ferromagnetic dots in three different lattice configurations as a function of separation between the dots. The "rigid vortex model" has been employed to determine the interaction energy of the coupled dots as a function of spacing between the dots. We have shown that by arranging the dots, in particular, configuration, the chirality of the vortex states in the dots can be controlled effectively by varying the direction of the applied field. We have further shown the existence of configurational anisotropy in the lattice geometries by studying the magnetization reversal behavior as a function of the applied field direction.

This work was supported by Ministry of Education (MOE) under Grant No. R-263-000-437-112 and the Singapore MIT Alliance. One of the authors (S.J.) would like to thank National University of Singapore (NUS).

*Corresponding author; eleaao@nus.edu.sg

[1] M. Natali *et al.*, J. Appl. Phys. **96**, 4334 (2004).
[2] J. I. Martin *et al.*, J. Magn. Magn. Mater. **256**, 449 (2003).
[3] A. O. Adeyeye and N. Singh, J. Phys. D **41**, 153001 (2008).
[4] A. Fernandez and C. J. Cerjan, J. Appl. Phys. **87**, 1395 (2000).
[5] R. P. Cowburn *et al.*, Phys. Rev. Lett. **83**, 1042 (1999).
[6] A. Lebib *et al.*, J. Appl. Phys. **89**, 3892 (2001).
[7] M. Natali *et al.*, Phys. Rev. Lett. **88**, 157203 (2002).
[8] K. Yu. Guslienko and K. L. Metlov, Phys. Rev. B **63**, 100403(R) (2001); K. Yu. Guslienko *et al.*, *ibid.* **65**, 024414 (2001); K. Yu. Guslienko, Phys. Lett. A **278**, 293 (2001).
[9] V. Novosad *et al.*, Phys. Rev. B **66**, 052407 (2002); V. Novosad *et al.*, *ibid.* **65**, 060402(R) (2002).
[10] J. Shibata *et al.*, Phys. Rev. B **67**, 224404 (2003); J. Shibata and Y. Otani, *ibid.* **70**, 012404 (2004).
[11] G. N. Kakazei *et al.*, Phys. Rev. B **74**, 060406(R) (2006).
[12] M. Grimsditch *et al.*, Phys. Rev. B **65**, 172419 (2002).
[13] V. Novosad *et al.*, Phys. Rev. B **72**, 024455 (2005).
[14] K. Yu. Guslienko and A. Hoffmann, Phys. Rev. Lett. **97**, 107203 (2006).
[15] J. I. Martin *et al.*, Phys. Rev. Lett. **79**, 1929 (1997).
[16] J. E. Villegas *et al.*, Phys. Rev. Lett. **99**, 227001 (2007).
[17] R. P. Cowburn, Phys. Rev. B **65**, 092409 (2002).
[18] R. P. Cowburn and M. E. Welland, Science **287**, 1466 (2000).
[19] A. Imre *et al.*, Science **311**, 205 (2006).
[20] X. Zhu and J.-G. Zhu, IEEE Trans. Magn. **39**, 2854 (2003).
[21] N. Singh *et al.*, Nanotechnology **15**, 1539 (2004).
[22] OOMMF framework available at http://math.nist.gov/oommf/.
[23] R. P. Cowburn *et al.*, Phys. Rev. Lett. **81**, 5414 (1998).